

Cite this article as: Song Bo, Xi Honglei, Fu Yu, et al. Influence of Pre-deformation on Phase Transformations and Microstructures in Near  $\beta$  Ti Alloy During Aging[J]. Rare Metal Materials and Engineering, 2024, 53(11): 3001-3009. DOI: 10.12442/j.issn.1002-185X.20240111.

ARTICLE

# Influence of Pre-deformation on Phase Transformations and Microstructures in Near $\beta$ Ti Alloy During Aging

Song Bo<sup>1,2</sup>, Xi Honglei<sup>2</sup>, Fu Yu<sup>2</sup>, Wang Junshuai<sup>2</sup>, Xiao Wenlong<sup>2,3</sup>, Ren Yanbiao<sup>4</sup>, Ma Chaoli<sup>2,3</sup>

<sup>1</sup>School of Materials Science and Engineering, Liaocheng University, Liaocheng 252059, China; <sup>2</sup>School of Materials Science and Engineering, Beihang University, Beijing 100191, China; <sup>3</sup>Tianmushan Laboratory, Hangzhou 310023, China; <sup>4</sup>College of Chemistry, Chemical Engineering and Materials Science, Zaozhuang University, Zaozhuang 277160, China

**Abstract:** The influence of pre-deformation on phase transformations, microstructures and hardening response in near  $\beta$  Ti alloy Ti-5Al-3Mo-3V-2Cr-2Zr-1Nb-1Fe (wt%) during aging treatment was studied. The results show that obvious  $\alpha$  phase refinement and stronger age hardening effect can be achieved when the alloy is slightly deformed before aging treatment. Because the formation of intermediate phases ( $O'$ ,  $\omega$  and  $O''$ ) suppresses long-range stress induced martensitic transformation and mechanical twinning, the alloy is mainly deformed via dislocation slipping during loading. Large numbers of crystal defects are generated during pre-deformation. With increasing the pre-deformation, the number density of dislocations increases gradually. These crystal defects generated by pre-deformation may partly annihilate upon early aging, but the precipitation of  $\alpha$  can also be promoted, resulting in refined  $\alpha$  precipitates. In the sample with 5% pre-strain, the average thickness of  $\alpha$  precipitates decreases by 57% after aging at 600 °C compared with the sample without pre-strain, and the number density increases from  $7.0 \pm 1$  laths/ $\mu\text{m}^2$  to  $22.0 \pm 3$  laths/ $\mu\text{m}^2$ . Some platelet-shaped  $\alpha$  phases form when the samples experience comparably large pre-strains such as 12% and 20%. It proves that the refined  $\alpha$  precipitates and better hardening effect can be achieved by pre-deformation plus aging treatment for titanium alloy.

**Key words:** titanium alloy; pre-deformation plus aging treatment; intermediate phases;  $\alpha$  precipitate

Near  $\beta$  Ti alloy has received considerable attention in aerospace field due to its high specific strength, good corrosion resistance and excellent hardenability for manufacturing landing gear, fasteners and other structural components<sup>[1-3]</sup>. These outstanding mechanical properties are primarily caused by  $\alpha$  precipitation in  $\beta$  matrix, which closely depends on morphology, size, volume fraction and distribution of  $\alpha$  phase<sup>[4-6]</sup>. Therefore, the influence of phase transformations kinetics on microstructures and mechanical properties of titanium alloy has become an attractive topic in recent years.

Numerous works are concentrated on controlling  $\alpha$  precipitation to achieve excellent mechanical properties by adjusting heat treatments, such as two-step aging treatments<sup>[7-9]</sup> and slow heating to aging temperatures<sup>[10-11]</sup>. In comparison with con-

ventional heat treatments, some investigations<sup>[12-16]</sup> confirm that refined microstructures and specific  $\alpha$  variant can be obtained via thermomechanical treatments, due to the effect of grain boundaries and crystal defects. These crystal defects generated by thermomechanical treatments, i.e., dislocations and vacancies, can significantly promote  $\alpha$  phase precipitation upon aging<sup>[17-20]</sup>. They provide additional preferential nucleation site for intragranular  $\alpha$  precipitates and facilitate  $\alpha$  growth. Dong et al<sup>[21]</sup> observed that plenty of dot-like  $\alpha$  precipitates are distributed non-uniformly nearby dislocations, and argued that the dislocations play a key role in the formation of V-shaped or triangular  $\alpha$  clusters. Liu et al<sup>[22]</sup> also reported the phenomenon of heterogeneous precipitation along the dislocations, which serve as effective nucleation

Received date: March 03, 2024

Foundation item: Natural Science Foundation of Shandong Province (ZR2022QE115); Liaocheng City Key Research Plan (2022YDSF85); Liaocheng University Doctoral Initiation Fund (318052132); Liaocheng University Students Innovation Plan (CXCY2023029); National Natural Science Foundation of China (51671012, 51671007, 52174346); International Science and Technology Cooperation Program of China (2015DFA51430); Aeronautical Science Foundation of China (2015ZF51069)

Corresponding author: Song Bo, Ph.D., Lecturer, School of Materials Science and Engineering, Liaocheng University, Liaocheng 252059, P. R. China, E-mail: songbo@buaa.edu.cn

Copyright © 2024, Northwest Institute for Nonferrous Metal Research. Published by Science Press. All rights reserved.

sites. Li et al.<sup>[23]</sup> discussed that the formation of ultrafine  $\alpha$  precipitates in cold-rolled and annealed sample is attributed to the fact that the high density of dislocations and vacancies accelerate  $\alpha$  transformation. It has been well known that the  $\beta \rightarrow \alpha$  transformation involves atom diffusion and displacive processes<sup>[24]</sup>. The diffusion of atoms insures required local composition for  $\alpha$  precipitation, and the displacive process contributes to lattice structure reconstruction of  $\alpha$  phase. During the structure reconstruction, dislocations and apparent transformation strains associated with  $\alpha$  precipitation appear. They can greatly affect the morphology characteristics of  $\alpha$  precipitates and variants selection<sup>[25-27]</sup>. Specific local microstructure can be formed to accommodate the external strain. For example, the  $\{112\}_\beta \langle 111 \rangle_\beta$  slip system is favor to the selection of  $\alpha$  variants with  $(1\bar{1}00)_\alpha$  parallel to the slip plane and the  $[11\bar{2}0]_\alpha$  parallel to the slip direction<sup>[21]</sup>. Hua et al.<sup>[28]</sup> found that in Ti-7Mo-3Nb-3Cr-3Al alloy, the  $\alpha$  precipitates in special regions have larger aspect ratio under isothermal compression treatments. Therefore, it is reasonable to suspect that the morphology characteristics of  $\alpha$  can be remarkably changed when pre-deformation is conducted before aging treatment. The strategy of imposing external strain or pre-strain prior to aging should be effective to control microstructures and to optimize mechanical properties.

Although the influence of crystal defects on  $\alpha$  variants selection has been investigated, the correlations between the number density of crystal defects and  $\alpha$  precipitate characteristics are still unclear. The underlying mechanisms of defects-assisted  $\alpha$  precipitation and mechanical properties improvement are not given. Hence, the objective of this work is to elucidate the impact of pre-deformation on phase transformations and microstructure evolution upon aging in titanium alloy.

## 1 Experiment

Initial material was supplied by Northwest Institute for Non-ferrous Metal Research, China<sup>[29]</sup>. The ingot was hot-rolled in  $\alpha + \beta$  zone temperature range into  $\Phi 20$  mm bars. Detailed chemical composition of this alloy has been reported<sup>[30]</sup>, which is Ti-5.02Al-3.03Mo-2.99V-2.06Cr-2.01Zr-1.37Nb-0.99Fe (wt%), named as Ti-5321. The  $\beta \rightarrow \alpha$  transformation temperature of Ti-5321 alloy is  $860 \pm 5$  °C, and its [Mo] is 6.06.

Solution treatment was performed at 900 °C for 0.5 h followed by water quenching. The as-quenched samples were slowly heated to 375 °C at 10 °C/min and water quenched. The pre-deformation of samples was realized by tensile deformation at a strain rate of  $4.63 \times 10^{-4}$  s<sup>-1</sup>, and different number densities of crystal defects were developed through changing the pre-strains, including 5%, 12%, 20% and 30%. To record the strains, an extensometer was loaded upon tensile tests. Electron back-scattered diffraction (EBSD) examinations were carried out for these strained samples using Oxford Nordly max3 system with HKL-Channel 5 software. The micro-hardness of samples was measured by Vickers hardness tester at a load of 0.98 N for 10 s. Ten points were tested to get the average values and error bars. Phase constituents were

analyzed by X-ray diffraction (XRD). For the aging treatment, pre-deformed samples were put into the furnace to preheat to 600 °C for 8 h followed by water quenching. Differential scanning calorimetry (DSC) measurements were conducted on Netzsch STA449F3 calorimeter at 10 °C/min to study phase transformations. The reflections of intermediate phases in  $\beta$  were simulated by CrystalMaker and SingleCrystal software. After aging at 600 °C, these samples were ground, polished and etched to reveal microstructures. Standard Kroll's reagent (10 mL HF+30 mL HNO<sub>3</sub>+70 mL H<sub>2</sub>O) was used to etch samples. The microstructures of samples were observed by JSM-6010 scanning electron microscope (SEM) and transmission electron microscope (TEM). TEM foils were prepared by twin-jet eletro-polishing under 30 V at -40 °C, and TEM observations were performed on JEM 2100 at 200 kV. The size and number density of  $\alpha$  precipitates were calculated by Image-Pro-Plus software.

## 2 Results

### 2.1 Initial microstructure

The microstructure of the  $\beta$ -quenched sample has been studied previously, in which plenty of equiaxed  $\beta$  grains with an average size of 185  $\mu$ m are developed. Within these  $\beta$  grains, intermediate phases O' and  $\omega$ -embryos exist. When the  $\beta$ -quenched sample is heated to 375 °C, a large number of parallel striations appear in  $\beta$  matrix, as shown by black contrast in bright field (BF) TEM image (Fig. 1a). This should be caused by  $\beta$  spinodal decomposition. Except for the diffractions of  $\beta$  phase, obvious reflections of intermediate phases are found in the selected area electron diffraction (SAED) pattern recorded along  $[113]_\beta$  direction (Fig. 1c). The reflections located at 1/3 and 2/3  $(2\bar{1}\bar{1})_\beta$  positions belong to isothermal  $\omega$  phase, which is referred by white contrast. The reflections located at 1/2  $(2\bar{1}\bar{1})_\beta$  positions and highlighted by yellow contrast come from the O' phase. The isothermal  $\omega$  phase is transformed by the  $\{1\bar{1}\bar{1}\}_\beta [1\bar{1}\bar{1}]_\beta$  collapse mixed with solute diffusion, and the development of O' is ascribed to the  $\{110\} \langle 1\bar{1}0 \rangle_\beta$  shuffle mechanism. By selecting the circled  $\omega$  reflections, the dark field (DF) TEM image (Fig. 1b) shows the uniformly distributed isothermal  $\omega$  precipitates with average diameter of 5 nm. It is noted that there are some additional reflections at 1/3 and 2/3  $(1\bar{1}0)_\beta$  positions, as highlighted by red contrast. In SAED patterns viewed along  $[001]_\beta$  (Fig. 1d) and  $[111]_\beta$  (Fig. 1e) directions, the reflections located at 1/3 and 2/3  $(1\bar{1}0)_\beta$  positions are also found. The phase diffraction intensity profile (Fig. 2) recorded along the dash line in Fig. 1d evidences clearly the existence of such additional reflections. These reflections are thought to come from O'' phase, and the identification of O'' phase is discussed in detail.

As reported in Ref. [31-33], the O'' phase has ordered face centered orthorhombic structure, and belong to Fmmm space group. Ordering occurs every three  $\{001\}_{O''}$  atom planes. To study the crystal structure of O'' phase in this alloy, TEM observations were performed, as shown in Fig. 3. Plenty of ellipsoidal O'' domains are uniformly distributed in  $\beta$  (Fig. 3a),

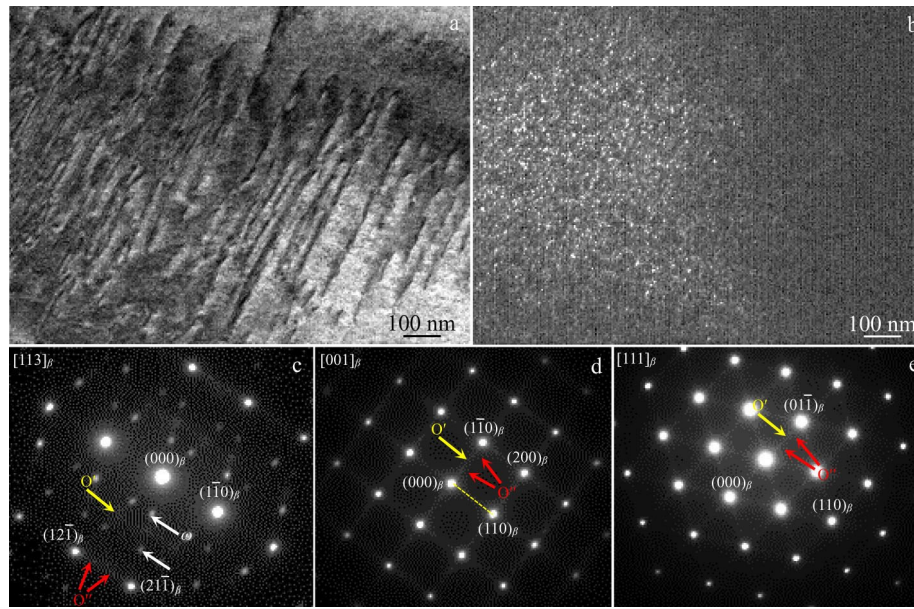


Fig.1 TEM images of Ti-5321 alloy slowly heated to 375 °C: (a) BF and (b) DF TEM showing the distribution of  $\omega$  particles; SAED patterns recorded along  $[113]_{\beta}$  (c),  $[001]_{\beta}$  (d), and  $[111]_{\beta}$  (e) directions

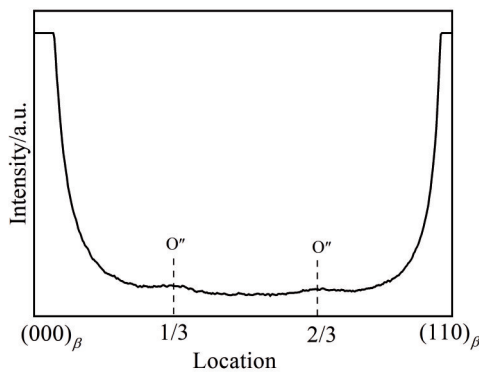


Fig.2 Intensity profile along the dash line between  $(000)_{\beta}$  and  $(110)_{\beta}$  marked in Fig.1d

and their average diameter is measured to be  $3 \pm 0.6$  nm. Based on SAED patterns, the orientation relationships between  $O''$  and  $\beta$  obey  $[100]_{\beta} // [100]_{O''}$ ,  $[110]_{\beta} // [010]_{O''}$ ,  $[111]_{\beta} // [110]_{O''}$  and  $[113]_{\beta} // [3\bar{1}0]_{O''}$ . Based on high-resolution TEM (HRTEM) observation, it is noted that the lattice parameters of  $O''$  are also closely related to that of  $\beta$  phase (Fig.3c), which obey  $a_{O''} = a_{\beta}$ ,  $b_{O''} = \sqrt{2}b_{\beta}$  and  $c_{O''} = 3\sqrt{2}c_{\beta}$ . The fast Fourier transformation (FFT) of the area circled by yellow dash lines and their corresponding inverse fast Fourier transformation (IFFT) patterns are also shown in Fig.3d and 3e, respectively. Using CrystalMaker and SingleCrystal software, the  $O''$  lattice structure is constructed (Fig. 3b), and the simulated SAED patterns along different directions are obtained (Fig.4). The  $O''$  reflections are indicated by red contrast, and the  $\beta$  reflections are indicated by black contrast. As discussed in Ref.[33], the formation of  $O''$  phase might be due to the Al atom enrichment in local regions. In titanium alloys, the content of Al elements should be lower than 6wt%, because short range

order and/or TiAl intermetallic compound will be formed once the Al content exceeds 6wt%. In this work, the Al content is 5wt% in Ti-5321 alloy. When the  $O''$  domains are developed accompanied by the  $O'$  and isothermal  $\omega$  precipitates, the Al atoms are excluded from  $O'$  and  $\omega$  precipitates during aging. This will lead to the Al atom enrichment in neighboring local regions, which is conducive to  $O''$  domain formation.

## 2.2 Pre-deformation of samples

Tensile curve and corresponding strain hardening rate curve of the sample heated to 375 °C are presented in Fig.5. It is noticed that there should be no mechanical twinning or stress induced phase transformations during deformation, because the activation of mechanical twins and/or stress induced phase transformations will result in abrupt increment of strain hardening rate during early deformation stage. The sample shows that typical dislocations slipping mechanism is dominated deformation behavior upon loading. The yield strength, ultimate tensile strength and fracture elongation of sample are  $862 \pm 5$  MPa,  $873 \pm 4$  MPa and  $30\% \pm 2\%$ , respectively. During tensile deformation at 5%–20% strain, the strain hardening rate is about 1 GPa.

Wu et al<sup>[34]</sup> has studied the deformation behavior of Ti-5321 alloy in  $\beta$ -quenched state, and argued that dislocations slipping, crystal rotation and stress induced  $\alpha''$  martensite transformation mechanisms dominate its deformation behavior. When slowly heated to 375 °C, three intermediate phases  $O'$ ,  $O''$  and isothermal  $\omega$  are formed. The  $O''$  phase with ordered structure can efficiently suppress the stress induced  $\alpha''$  martensite transformation. Combined with the effect of  $O'$  and isothermal  $\omega$ , the sample should deform primarily through dislocation slipping. The interactions of these intermediate phases with dislocations upon loading are unclear, which will be studied in future.

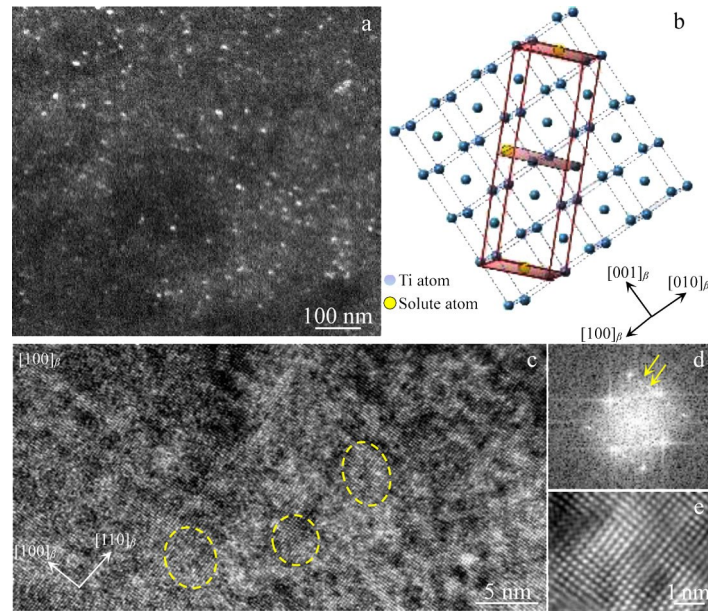


Fig.3 DF TEM image of O'' domain distribution (a); schematic illustration of the structure of  $\beta$  with O'' cell (b); HRTEM image of the lattice structure in O'' domains (c); FFT (d) and IFFT (e) patterns of the circled regions in Fig.3c

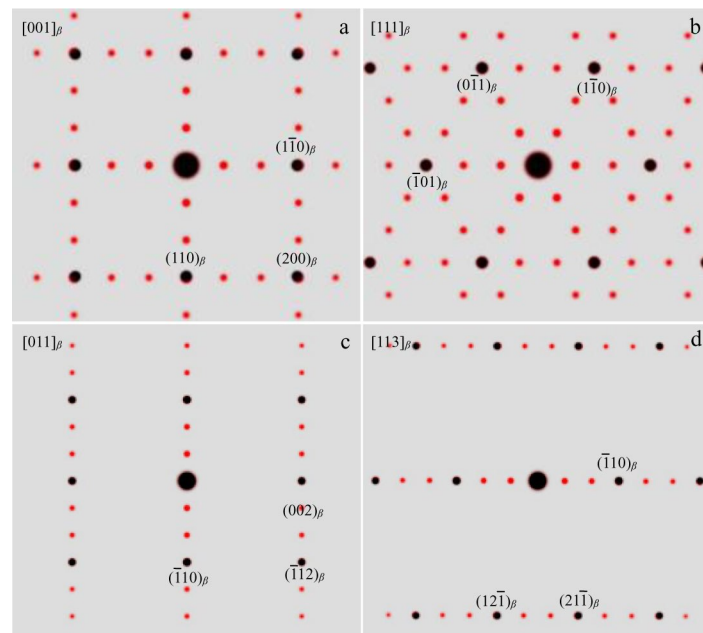


Fig.4 Simulated SAED patterns of O'' in  $\beta$  phase along  $[001]_{\beta}$  (a),  $[111]_{\beta}$  (b),  $[011]_{\beta}$  (c), and  $[113]_{\beta}$  (d) directions

To clarify the deformation mechanisms of this sample, the microstructure in regions nearby fracture surface is carefully studied. XRD patterns (Fig.6) show that there is only  $\beta$  phase after fracture without  $\alpha''$  martensite. The phase constituents of sample before tensile deformation are also given for comparison. It evidences that the sample is actually deformed via dislocations slipping mechanism. To investigate the influence of dislocations on promoting  $\alpha$  precipitation, the samples were pre-deformed to various tensile strains, as shown in Fig.7. At pre-strain of 5%, the dislocation traces in two directions can be clearly found (Fig. 7b). With further

increasing the strain, the number density of dislocation traces is greatly increased, as shown in Fig.7c–7d. These deformed microstructures are further analyzed by EBSD, and it is found that no twins or stress induced phase transformations appear within  $\beta$  grains. In the sample with 5% pre-strain, parallel dislocation traces are observed in the inverse pole figure (IPF) and image quality (IQ) map, as shown in Fig.8a–8b, and the phase map shows that there is only  $\beta$  phase without  $\alpha''$  martensite (Fig.8c). Similar observations are also found in the sample with 20% pre-strain (Fig. 9). Plenty of parallel dislocation slipping traces are observed. Even though there is

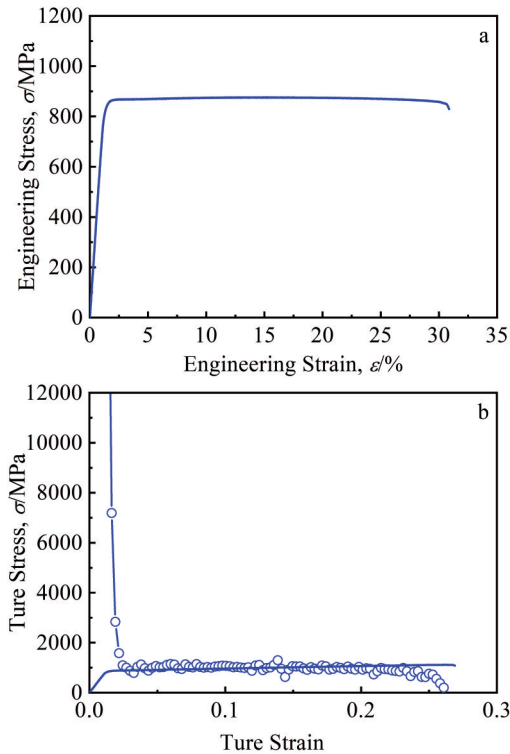


Fig.5 Engineering stress-engineering strain curve of the sample heated to 375 °C (a) and corresponding true stress-true strain and strain hardening rate curves (b)

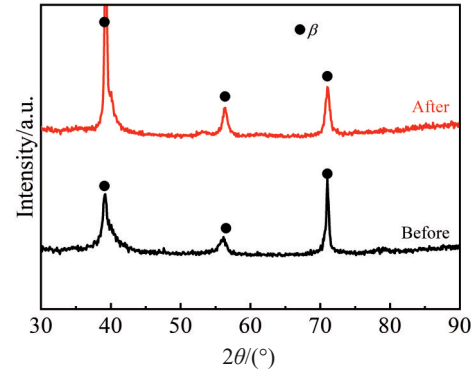


Fig.6 XRD patterns of tensile samples before and after deformation

larger number density of dislocations in the IPF and IQ map shown in Fig. 9a–9b, no twins or  $\alpha''$  martensite appear. The corresponding phase map (Fig. 9c) presents only  $\beta$  phase without  $\alpha''$  martensite. For the deformed samples, the local strain is primarily accommodated by the dislocations slipping, as indicated by their corresponding kernel average misorientation (KAM) maps (Fig.8d and Fig.9d).

### 2.3 $\alpha$ precipitation upon aging

Fig. 10 shows the microstructures of samples with various pre-strains after aging at 600 °C. A dense and uniform distribution of  $\alpha$  precipitates can be observed in all samples, and slight deformation prior to aging treatment is beneficial to

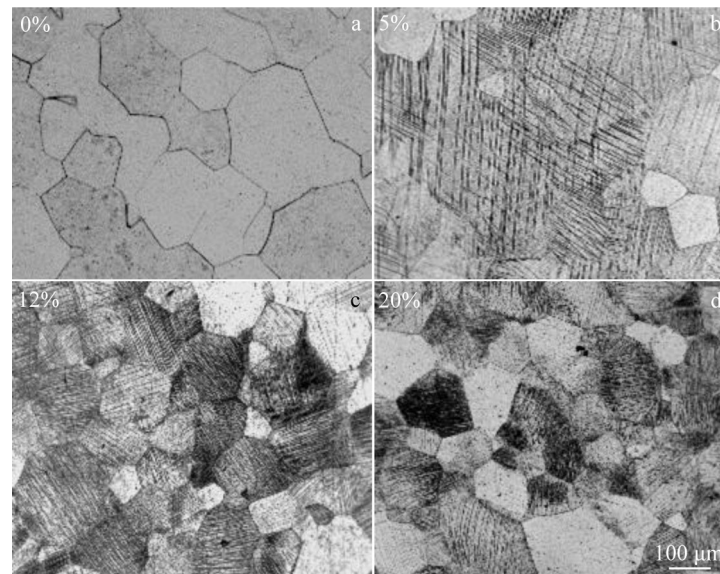


Fig.7 Microstructures of samples with pre-strains of 0% (a), 5% (b), 12% (c), and 20% (d)

microstructures refinement. Compared with the undeformed sample (Fig. 10a),  $\alpha$  precipitates have smaller size and larger number density in these deformed samples. With 5% pre-strain (Fig. 10b), the average length and thickness of  $\alpha$  precipitates drop from  $0.67\pm 0.23$  and  $0.14\pm 0.02$   $\mu\text{m}$  to  $0.25\pm 0.02$  and  $0.06\pm 0.01$   $\mu\text{m}$ , respectively (57% reduction in thickness). The number density of  $\alpha$  precipitates greatly increases from  $7.0\pm 1$  laths/ $\mu\text{m}^2$  to  $22.0\pm 3$  laths/ $\mu\text{m}^2$ . The

features of  $\alpha$  precipitates in samples with various pre-strains are summarized in Table 1. It is worth noting that the thickness and number density of  $\alpha$  precipitates seem to be unchanged, and the length and aspect ratio decrease continually with increasing the pre-strain. To characterize the morphology changing of  $\alpha$  phase, the microstructures of samples with 5% and 20% pre-strains are comparatively studied, as shown in Fig.11. In the sample with 5% pre-strain,

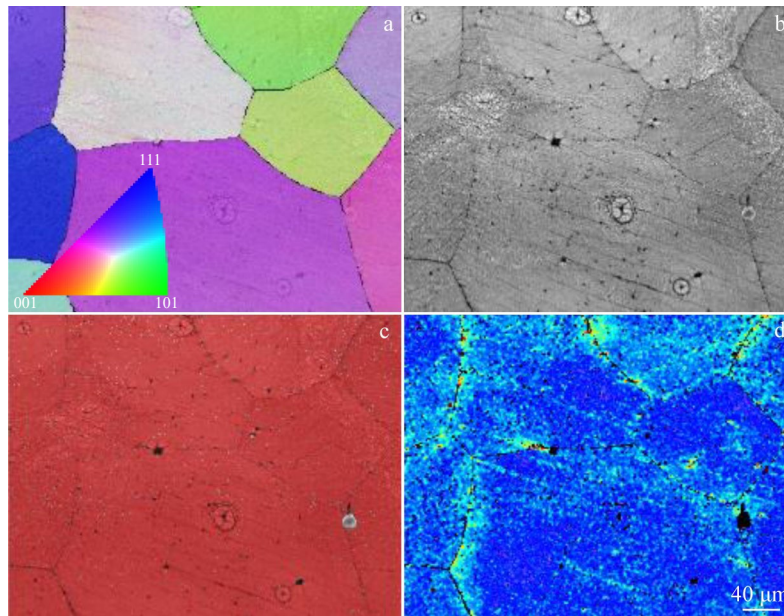


Fig.8 IPF map (a), IQ map (b), phase map (c), and KAM map (d) of sample with 5% pre-strain

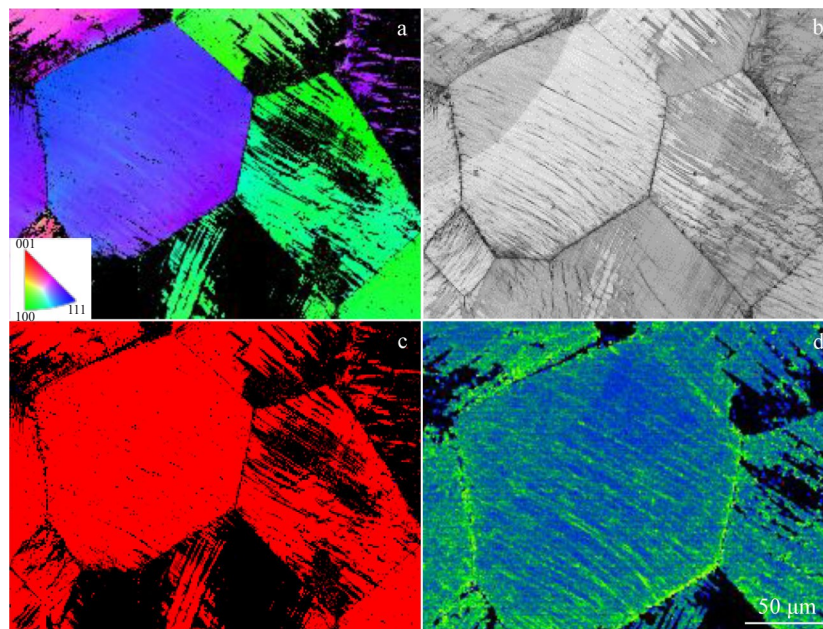


Fig.9 IPF map (a), IQ map (b), phase map (c), and KAM map (d) of sample with 20% pre-strain

the aspect ratio of  $\alpha$  phase is  $4.2 \pm 1$ , and it is reduced to  $2.3 \pm 1.2$  in the sample with 20% pre-strain. This suggests that the pre-deformation facilitates  $\alpha$  precipitate globularization upon aging.

In the samples with 12% and 20% pre-strains, a large number of platelet-shaped  $\alpha$  phases with large aspect ratio are noticed, as indicated by red arrows (Fig. 10c – 10d). Dislocations of large number density should be generated in such two samples after pre-deformation, and they can reduce  $\alpha$  phase nucleation energy barrier and facilitate  $\alpha$  growth along the dislocations direction. When the  $\alpha$  phase nucleates

at dislocations during aging, it may grow up along the dislocations, leading to formation of platelet-shaped  $\alpha$  phase. Therefore, the platelet-shaped  $\alpha$  formation should be caused by the number of dislocations upon pre-deformation.

Micro-hardness of the samples with various pre-strains after aging at 600 °C is given in Fig.12. With increasing the strain, the micro-hardness of alloy increases gradually, and the minimum and maximum values are obtained when the pre-strains are 0% and 30%, respectively. For the sample without pre-strain, its micro-hardness is measured to be  $2058.0 \pm 49.0$  MPa. While the micro-hardness of sample with 30% pre-strain

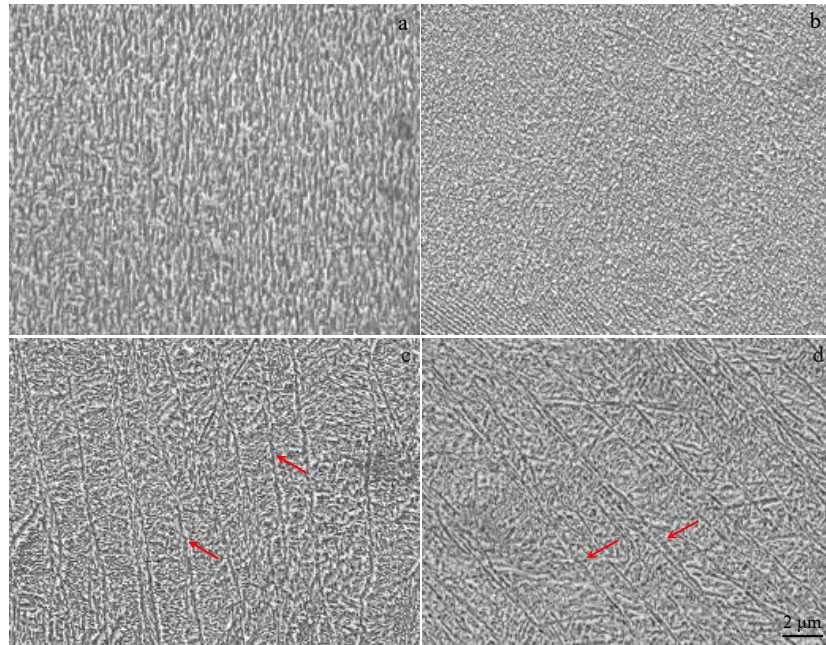


Fig.10 SEM images of samples with different pre-strains after aging at 600 °C: (a) 0%, (b) 5%, (c) 12%, and (d) 20%

**Table 1** Features of  $\alpha$  precipitates in samples with different pre-strains after aging at 600 °C

Parameter	0%	5%	12%	20%
Length/ $\mu\text{m}$	$0.67\pm 0.23$	$0.25\pm 0.02$	$0.19\pm 0.03$	$0.16\pm 0.05$
Thickness/ $\mu\text{m}$	$0.14\pm 0.02$	$0.06\pm 0.01$	$0.07\pm 0.02$	$0.07\pm 0.02$
Aspect ratio	$4.8\pm 2.5$	$4.2\pm 1.0$	$2.7\pm 1.3$	$2.3\pm 1.2$
Number density/laths $\cdot\mu\text{m}^{-2}$	$7.0\pm 1.0$	$22.0\pm 3$	$21.0\pm 2.0$	$24.0\pm 2.0$

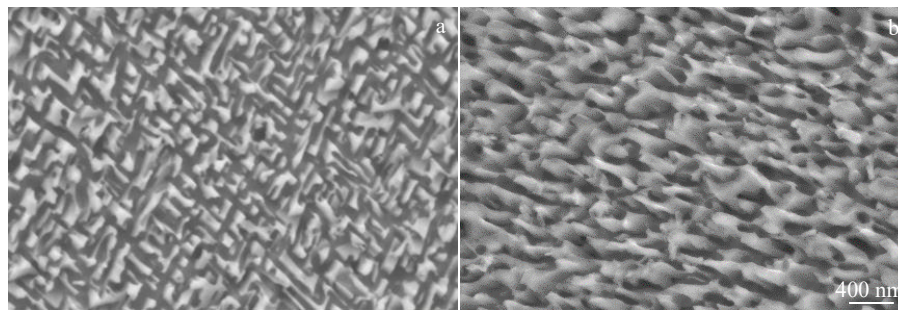


Fig.11 Comparison of  $\alpha$  precipitates in samples with pre-strains of 5% (a) and 20% (b)

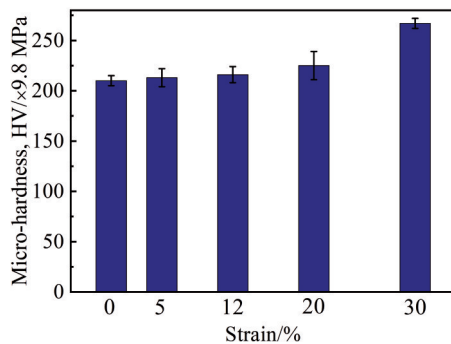


Fig.12 Micro-hardness of samples with different pre-strains after aging at 600 °C

increases up to  $2616.6\pm 88.2$  MPa. This suggests that the crystal defects induced by pre-deformation can actually result in larger age hardening effect.

### 3 Discussion

DSC curves of the samples with different pre-strains during slow heating at  $10\text{ }^{\circ}\text{C}/\text{min}$  are shown in Fig.13. It is noted that these samples experience the same phase transformation sequences. For the sample with 5% pre-strain, the  $\alpha$  precipitation occurs from  $365\text{ }^{\circ}\text{C}$  to  $457\text{ }^{\circ}\text{C}$ . Before the exothermic peak of  $\alpha$  precipitation, there is an endothermic event at  $319\text{--}362\text{ }^{\circ}\text{C}$ , which should be caused by the recovery of sample and dislocations annihilation. With increasing the

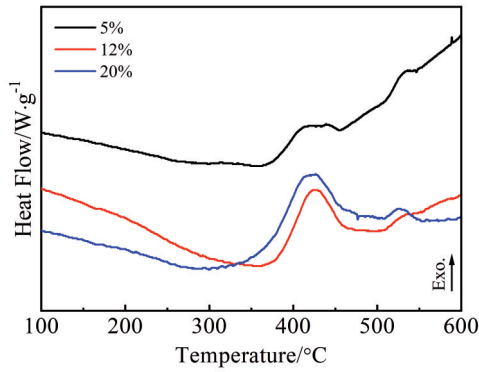


Fig.13 DSC curves of samples with different pre-strains during heating at 10 °C/min

strain, the  $\alpha$  precipitation temperature range is not affected, but the temperature of dislocations annihilation is obviously reduced. When the strain increases to 12%, the temperature of such endothermic peak decreases to 202 °C. For the sample with 20% pre-strain, it is further reduced to 196 °C. The enthalpy value of endothermic reaction in samples with 12% and 20% pre-strains is apparently larger than that in sample with 5% pre-strain.

It is argued that the nucleation of  $\alpha$  phase is mainly via  $O'$ -assisting mechanism upon aging in Ti-5321 alloy, and the  $O'$  can also be transformed to  $\alpha$  colonies directly<sup>[35-37]</sup>. Based on the results above, it can be known that the dislocations can effectively refine  $\alpha$  precipitates during aging and result in higher micro-hardness (Fig.12). To study the precipitation of  $\alpha$  phase, TEM observations are performed. When the pre-deformed sample is heated to 430 °C at 10 °C/min, a large

number of  $O'$  domains co-exist with  $\alpha$  needles (Fig.14). This evidences that  $\alpha$  precipitation is indeed via  $O'$ -assisted nucleation mechanism.  $\alpha$  needles tend to form at the  $O'$  phase interfaces. It has been accepted that the intermediate phases do not necessarily act as the precursor of  $\alpha$ , which reduces the energy barrier for  $\alpha$  nucleation by acting as favorable nucleation sites<sup>[38]</sup>.

As the pre-strain is increased from 0% to 5%, apparent refinement of  $\alpha$  precipitates occurs in the aged samples, the average thickness of  $\alpha$  precipitates decreases from  $0.67\pm 0.23$   $\mu\text{m}$  to  $0.25\pm 0.02$   $\mu\text{m}$ , and the number density increases from  $7.0\pm 1$  laths/ $\mu\text{m}^2$  to  $22.0\pm 3$  laths/ $\mu\text{m}^2$ . This indicates that the tensile deformation before aging treatment is actually effective to refine microstructures and to improve mechanical properties, which is consistent with other works<sup>[18-19]</sup>. When such pre-strain further climbs to 12%, the thickness and number density of  $\alpha$  phase have little changes. Detrimental platelet-shaped  $\alpha$  phase is formed, leading to mechanical anisotropy in samples. It is thought that most dislocations induced by pre-deformation will annihilate and disappear before  $\alpha$  precipitation during aging, leading to obvious endothermic reaction prior to  $\alpha$  transformation. Therefore, it is thought that these dislocations might play both direct and indirect roles in affecting  $\alpha$  phase nucleation and growth. The dislocations may promote the formation of intermediate phases upon early aging and generate more heterogeneous site for  $\alpha$  precipitation. For the Ti-5321 alloy, it is suspected that the dislocations promote the development of  $O'$  domains during early aging stage, and the  $\alpha$  precipitation is promoted. The influence of  $O'$  phase on promoting  $\alpha$  nucleation behavior has been discussed in detail in other work<sup>[37]</sup>.

## 4 Conclusions

1) Since the development of intermediate phases  $O'$ ,  $\omega$  and  $O''$  suppresses stress induced martensitic transformation and mechanical twinning, the sample of Ti-5321 alloy deforms mainly through dislocations slipping mechanism. With increasing the prestrain, the amount of crystal defects increases gradually. These pre-deformed samples experience the same phase transformations during aging.

2) In comparison with sample without pre-deformation, obvious  $\alpha$  refinement and larger hardening effect are realized by the pre-deformation plus aging treatment. For the sample with 5% pre-strain, the average thickness of  $\alpha$  precipitates is reduced by 57% after aging at 600 °C, and the number density is increased from  $7.0\pm 1$  laths/ $\mu\text{m}^2$  to  $22.0\pm 3$  laths/ $\mu\text{m}^2$ .

3) The  $\alpha$  precipitates nucleate via the  $O'$ -assisted mechanism during aging in Ti-5321 alloy. The crystal defects generated by pre-deformation can effectively promote the formation of intermediate phases upon early aging and provide more heterogeneous nucleation sites for  $\alpha$  precipitates.

## References

- 1 Zhao Yongqing, Sun Qiaoyan, Xin Shewei et al. *Materials Science and Engineering A[J]*, 2022, 845: 143260

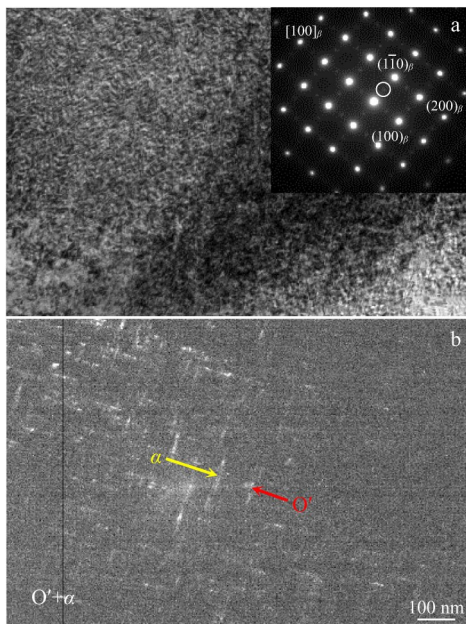


Fig.14 BF TEM image of the sample with 5% pre-strain heated to 430 °C with the inset SAED pattern along  $[100]_{\beta}$  direction (a); DF TEM image showing co-existence of  $O'$  and  $\alpha$  (b)

- 2 Anil Kumar V, Gupta R K, Prasad M J N V. *Journal of Materials Research*[J], 2021, 36: 689
- 3 Dipankar B, Williams J C. *Acta Mater*[J], 2013, 61: 844
- 4 Zhu X J, Han F, Wang D et al. *Journal of Alloys and Compounds*[J], 2023, 933: 167758
- 5 Zhang T, Huang H, Hosseini S R E et al. *Materials Science and Engineering A*[J], 2022, 835: 142624
- 6 Zhang H, Zhang J, Liu S et al. *Acta Mater*[J], 2023, 255: 119082
- 7 Xu Y, Liu H, Zhang S et al. *Journal of Materials Research and Technology*[J], 2022, 18: 2870
- 8 Salvador C A F, Opini V C, Mello M G et al. *Materials Science and Engineering A*[J], 2019, 743: 716
- 9 Mantri S A, Choudhuri D, Alam T et al. *Scr Mater*[J], 2018, 154: 139
- 10 Zhang J, Ju H, Xu H et al. *Journal of Materials Science & Technology*[J], 2021, 94: 1
- 11 Mello M, Dainese B, Caram Rubens et al. *Mater Charact*[J], 2018, 145: 268
- 12 Zhu Z, Liu Y, Chen Z et al. *China Foundry*[J], 2023, 20: 23
- 13 Dan A, Cojocaru E M, Raducanu D et al. *Journal of Materials Research and Technology*[J], 2022, 19: 2877
- 14 Wang S, Liang Y, Sun H et al. *Materials Science and Engineering A*[J], 2021, 812: 141095
- 15 Naydenkin E V, Mishin I P, Oborin V A et al. *Materials Letters*[J], 2021, 300: 130132
- 16 Hua K, Zhang Y, Zhang F et al. *Materials Characterization*[J], 2021, 181: 111505
- 17 Hua K, Zhang Y, Gan W et al. *Acta Mater*[J], 2018, 161: 150
- 18 Wan M, Zhao Y, Zeng W et al. *Journal of Alloys and Compounds*[J], 2015, 619: 383
- 19 Han Wen, Fu Li, Chen Haiyan et al. *Rare Metal Materials and Engineering*[J], 2018, 47(8): 2335 (in Chinese)
- 20 Song Z Y, Sun Q Y, Xiao L et al. *Materials Science and Engineering A*[J], 2010, 527: 691
- 21 Dong R, Kou H, Zhao Y et al. *Journal of Materials Science & Technology*[J], 2021, 95: 1
- 22 Liu C, Hu X, Qi L et al. *Acta Mater*[J], 2023, 242: 118466
- 23 Li T, Kent D, Sha G et al. *Materials Science and Engineering A*[J], 2014, 605: 144
- 24 Hua K, Zhang Y, Kou H et al. *Acta Mater*[J], 2017, 132: 307
- 25 Hua K, Zhang Y, Gan W et al. *Acta Mater*[J], 2018, 161: 150
- 26 Qiu D, Shi R, Zhang D et al. *Acta Mater*[J], 2015, 88: 218
- 27 Shi R, Wang Y. *Acta Mater*[J], 2013, 61: 6006
- 28 Hua K, Zhang F, Kou H et al. *Progress in Natural Science: Materials International*[J], 2021, 31: 471
- 29 Xin Shewei, Zhao Yongqing, Zeng Weidong. *Rare Metal Materials and Engineering*[J], 2008, 37(3): 423 (in Chinese)
- 30 Ren Lei, Xiao Wenlong, Chang Hui et al. *Materials Science and Engineering A*[J], 2017, 711: 553 (in Chinese)
- 31 Antonov S, Shi R, Li D et al. *Scr Mater*[J], 2021, 194: 113672
- 32 Zheng Yufeng, Antonov Stoichko, Feng Qiang et al. *Scr Mater*[J], 2020, 176: 7
- 33 Zheng Y F, Williams R E A, Fraser H L. *Scr Mater*[J], 2016, 113: 202
- 34 Wu Cong, Zhao Yongqing, Huang Shixing et al. *Journal of Materials Science Technology*[J], 2022, 112: 36
- 35 Song Bo, Chen Yu, Xiao Wenlong et al. *Materials Science and Engineering A*[J], 2020, 793: 139886
- 36 Song Bo, Xiao Wenlong, Fu Yu et al. *Mater Letts*[J], 2020, 275: 128147
- 37 Li T, Lai M, Kostka A et al. *Scr Mater*[J], 2019, 170: 183
- 38 Li Dongdong, Wan Weifeng, Zhu Lvqi et al. *Acta Mater*[J], 2018, 151: 406

## 预变形对近 $\beta$ 钛合金时效阶段的相变及微观组织影响

宋 博<sup>1,2</sup>, 郗洪雷<sup>2</sup>, 付 雨<sup>2</sup>, 王俊帅<sup>2</sup>, 肖文龙<sup>2,3</sup>, 任衍彪<sup>4</sup>, 马朝利<sup>2,3</sup>

(1. 聊城大学 材料科学与工程学院, 山东 聊城 252059)

(2. 北京航空航天大学 材料科学与工程学院, 北京 100191)

(3. 天目山实验室, 浙江 杭州 310023)

(4. 枣庄学院 化学工程与材料科学学院, 山东 枣庄 277160)

**摘 要:** 研究了预变形对近 $\beta$ 钛合金 Ti-5Al-3Mo-3V-2Cr-2Zr-1Nb-1Fe (质量分数, %) 在时效处理中相变、微观组织及强化响应的影响。结果表明, 合金经预变形后再进行时效处理可以获得明显细化的 $\alpha$ 相与更好的时效强化效果。由于中间相 $O'$ 、 $\omega$ 和 $O''$ 的形成抑制了长程应力诱导马氏体相变机制和机械孪晶, 合金变形主要是通过位错滑移机制。预变形过程中会产生大量晶格缺陷, 随着预变形量的增大, 位错数量密度逐渐上升。这些由预变形产生的晶格缺陷会在时效初期部分湮灭, 但是仍然能够促进 $\alpha$ 相析出, 实现 $\alpha$ 相细化。与未预变形的样品相比, 预变形量为5%的样品在600 °C时效后 $\alpha$ 相的平均宽度会下降57%, 而且数量密度由 $7.0 \pm 1 \text{ laths}/\mu\text{m}^2$ 上升至 $22.0 \pm 3 \text{ laths}/\mu\text{m}^2$ 。当预变形量较大时, 如12%和20%, 会形成板条状的 $\alpha$ 相, 这说明钛合金经预变形后再时效处理可以获得细化的 $\alpha$ 相与更好的强化效果。

**关键词:** 钛合金; 预变形与时效处理; 中间相;  $\alpha$ 析出相